Automated visual inspection of particle defect in semiconductor packaging

Joonsub Park[1] and Jeonghoon Lee[1,2]

[1]Department of Mechanical Engineering, Graduate School, Korea University of Technology and Education, Cheonan-si, Korea, [2]School of Mechanical Engineering, Korea University of Technology and Education, Cheonan-si, Korea

Abstract   In semiconductor production processes, controlling and inspecting contamination particle defects are extremely important because even a small particle within any stage of the process can remarkably affect the quality of the final products. Particle contamination can be critically detrimental in every process, thereby reducing production yield in semiconductor processes. In this study, we investigated the correlation between the actual defect rate and the probability of contamination particle defect observed by a commercially available automated visual inspection (AVI) system in semiconductor backend processes. During mass production, we observed that contamination particles produced in a thermal process were transported to various locations and caused defects. Particles sized 45 μm were observed most frequently compared with the actual contamination particles and AVI images. To effectively detect particle defect on wafer surfaces, particles smaller than 100 μm should also be considered. The hallmark of this study is that we effectively controlled particles larger than 50 μm using our AVI equipment after the die attach approach to reduce defects in the wire bonding process in advance. We provide monitoring methods for contamination control of particles present in the thermal process on the AVI system applied in mass production processes. Finally, we suggest a plausible entrainment pathway of the contamination particles and present visual images of actual contamination particles observed using an optical microscope.

1. Introduction

Novel packaging technology is required to satisfy the preferences of consumers for small and feature rich electronic products, driving the miniaturization and high performance of electronic components [1]. Semiconductor technology has continuously increased the density of semiconductor chips due to advance in technology, such as lithography, as well as package, particularly the increase in semiconductor chip stacking density and the reduction in solder ball pitch spacing [2]. The risk of defects associated with particles naturally increases as semiconductor packaging products continue to diminish. In fact, the occurrence rate of defects caused by particles in semiconductor packaging processes has been steadily increasing. The continuous increase in the defect occurrence rate due to particles can be attributed to the high complexity of semiconductor packaging, which primarily involves mechanical processing driven by various moving parts, leading to the inevitable particle generation. In addition, subsequent steps involve thermal processes, simplifying the transport of particles. Particles that adhere to the chip and the substrate can become embedded, leading to defects. Contamination particles adhere to the chip and the substrate surface due to electrostatic forces, van der Waals forces, electrostatic double layer formation, capillary force, and chemical bonding between particles and surfaces [3]. Applying an air jet inside the semiconductor packaging equipment by optimizing conditions, such as distance and flow rates, is an appropriate approach to eliminate defects. This optimization increases the velocity of particles on the chip surface during cleaning, thereby enhancing particle cleaning efficiency [4]. Another technique is to clearly define the level of particle defects, identify the origins of each defect, and then fundamentally remove them to

prevent their occurrence [5]. Usually, data generated from particle defects classify the types of defects, calculate particle defect rates, analyze the defect components based on the severity, and trace the equipment causing defects. When deep learning algorithms, such as the convolutional neural network, are utilized, the defect component analysis may be skipped and directly predict the defect components [6]. However, this method can be costly and often impossible to shut down production facilities to investigate the cause of defects when detected in a semiconductor production environment. Usually, a large number of production plans are primarily scheduled in advance. Thus, switching to downtime for equipment inspection becomes economically unfeasible. Consequently, halting the equipment becomes challenging without relying on highly accurate results. The most appropriate analysis methods that consider the production environment must be applied to overcome the challenges in defect analysis within such restrictions regarding production environment and to enhance the accuracy of analysis. For example, non-destructive electronic speckle pattern interferometry was used to evaluate internal defects of semiconductor packages quantitatively [7]. In addition, data acquisition systems suitable for the production process of compound semiconductors were designed and built by analyzing the characteristics of the compound semiconductor fabrication process [8].

In this study, we investigate the particle defects developed in the process of using automated visual inspection (AVI) [9] equipment placed between the process steps. The shapes of actual particle defects are observed through a scanning electron microscope, and their size distribution is obtained by image analysis. The relationship between the actual defect rate and the AVI detection rate in a thermal process is investigated to determine factors contributing to particle defect and suggest the necessity of particle monitoring by using the AVI system for detecting particle defects in advance.

2. Methods

2.1 Packaging process and particle defect

Semiconductor packaging processes involve the assembly of wafers into packages, testing, and the shipment of the final products, as shown in Fig. 1. Typically, in back lapping, silicon wafer without patterns on the back is ground to reduce its thickness. In sawing, the wafer is cut into individual chips. In die attach, these divided chips are transported and attached to a substrate. The wire bonding process connects the chip pad to the substrate pad using gold wires. The chips are then protected with epoxy molding compound and are marked on the molding surface during marking. Subsequently, solder balls are attached to the substrate's back pads. The process is competed with sorting, where substrates are cut into individual packages, assembly, characteristic testing, and product shipment to customers.

We performed the wire bonding process to investigate parti-

Table 1. Specification of AVI equipment.

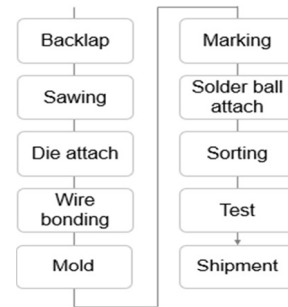| Method	Pixel resolution	Field of view	Camera specification
2D line scan	7 µm/pixel	30 mm	8K line scan

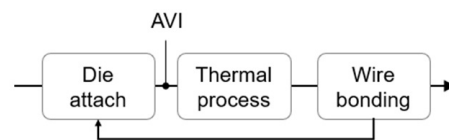Fig. 1. Schematic of packaging process.

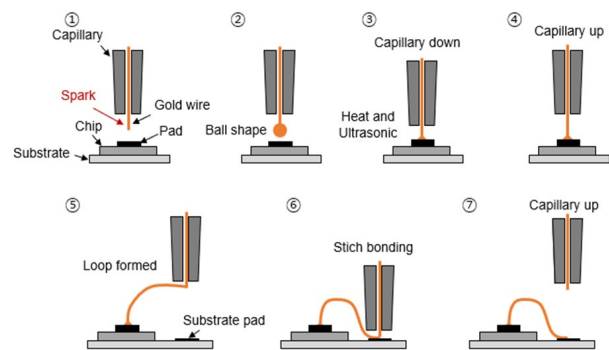Fig. 2. Particle inspection after die attach and prior to wire bonding.

Fig. 3. Schematic of the wire bonding sequence.

cle defects given the high defect rates in this step among the other processes in the entire semiconductor packaging. The typical process flow prior to wire bonding involves the following sequential steps shown in Fig. 2: die attach [10] → thermal process [11] → wire bonding [12]. During the die attach process, chips in wafer form are attached to the substrate. Subsequently, in wire bonding, the pads on the chip are connected to those on the substrate using gold wire after the thermal process of heat treatment. Particle defect is monitored using the AVI equipment after the die attach process. The specifications of the AVI equipment are detailed in Table 1. While variations may be observed depending on the chip stack structure, the process sequence described earlier is repeated as the number of chips on the substrate increases.

The wire bonding process is detailed to understand how particle defects are created in the backend process, as shown in
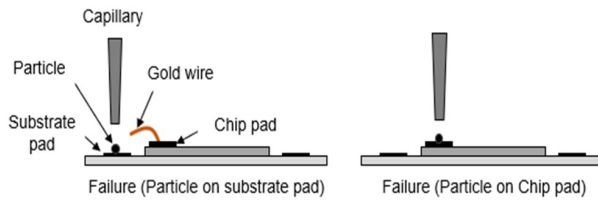
Fig. 4. Particle defect in wire bonding.

Fig. 5. Image of chip pad and substrate pad observed with scanning electron microscope.

Fig. 3. Initially, a capillary filled with gold wire at the center is prepared to initiate wire bonding. Then, a ball shape is formed on the gold wire of the capillary using spark. The capillary then moves down to connect the chip pad to the gold wire using heat and ultrasonic. The capillary moves up again to create a loop formation, followed by a stitch bonding to connect the gold wire to the substrate pad. This approach represents a typical wire bonding, where the gold wire is connected to the chip pad and the substrate pad, thereby completing the process.

Particles can be generated due to friction or wear of the drive components in the die attach process, which involves frequent mechanical motion. As shown in Fig. 4, particles generated in the die attach process subsequently fall onto the chip area and proceed to the subsequent processes. During the wire bonding process, particles adhere on the substrate pad or the chip pad. This condition can lead to defect because the capillary cannot establish appropriate wire connections.

Particle defects are observed in wire bonding. However, the particles can already be generated in the die attach process. Therefore, after the die attach process, we utilized AVI equipment in the subsequent step to monitor and analyze contamination particles. Typically, using an AVI equipment for particle monitoring is highly desirable. However, the most challenging aspect is to determine the criteria for monitoring particles in terms of their size. We categorized defective particles by size and examined product defects for different particle sizes to establish a reliable method to manage defects for size criteria using our AVI equipment, considering the resolution of vision part of the equipment.

3. Results and discussion

3.1 Observation of substrate pad, chip pad, and gold wire

As shown in Fig. 5, the diameter of the gold wire used in the wire bonding process was approximately 20 μm. The widths of the chip pad and the substrate pad were observed to be in the range of approximately 50 μm to 100 μm. In addition, the uncertainty of the measurement at approximately 6.5 % is determined from the image resolution. The detected particle size in the AVI was categorized into four groups, considering the gold wire diameter and the widths of the chip pad and the substrate pad. The small size group ranges from 20 μm to 50 μm. Middle 1 size group ranges from 50 μm to 100 μm. Middle 2 size group ranges from 100 μm to 150 μm, and large-size group
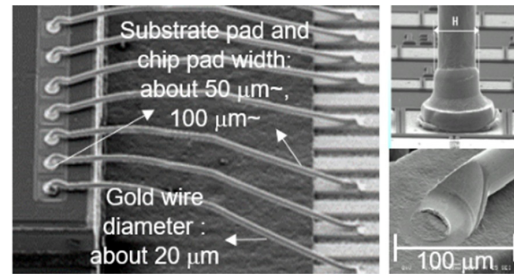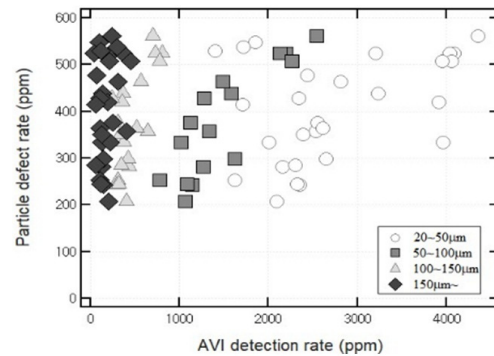

Fig. 6. Correlation between particle defect rate and AVI detection rate.

includes sizes greater than 150 μm. Correlation analysis was performed for each group with wire bonding defects.

3.2 Correlation analysis

We have presented four groups of detection with AVI using particle size and the corresponding defect rates occurring in the wire bonding process, as shown in Fig. 6. The x-axis represents the AVI detection rate, indicating the number of particles detected by the AVI equipment as defects, and the y-axis illustrates the particle defect rate, suggesting the quantity of defective particles in the actual wire bonding. The AVI detection rate and the particle defect rate are expressed in parts per million (ppm). The correlation between the AVI detection rate and the particle defect rate was confirmed by conducting the linear regression analysis using the AVI detection and the particle defect rates. In Eq. (1), ε represents the particle defect rate, and μ represents the number of wire bonding defective particles, obtained using the number of faulty chips during wire bonding. In the equation, γ represents the wire bonding population parameter, which is the total number of chips in wire bonding. In Eq. (2), α represents the AVI detection rate, ρ represents the wire bonding population parameter, and β represents the AVI population parameter.

$$\varepsilon = \frac{\mu}{\gamma} \times 10^6 \qquad (1)$$

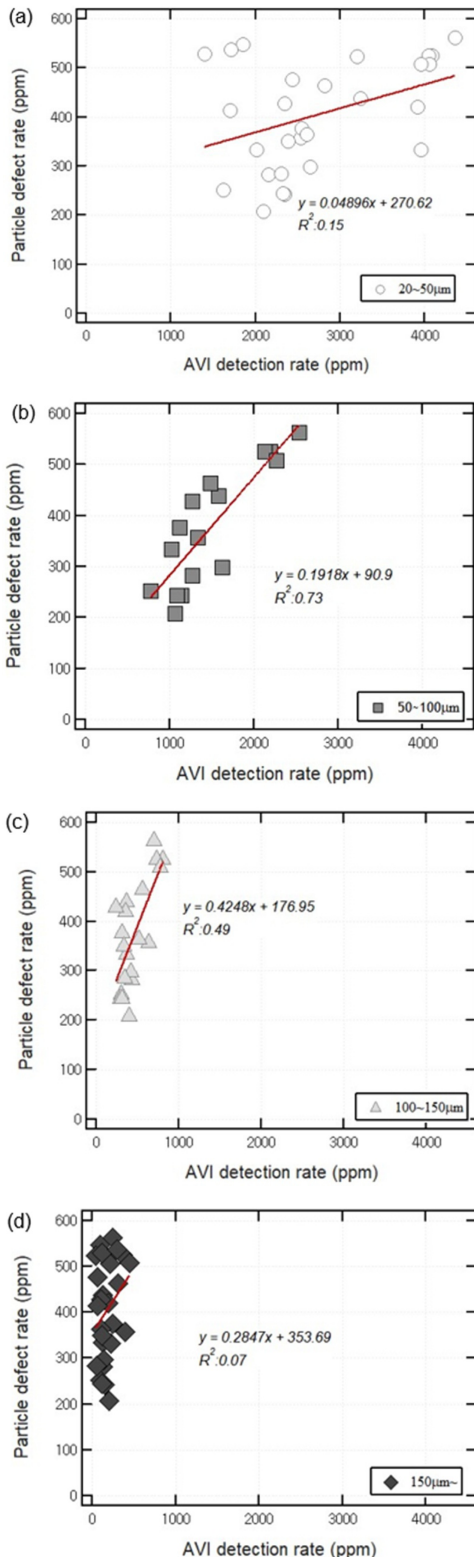$$\alpha = \frac{\rho}{\beta} \times 10^6 \qquad (2)$$

Fig. 7. Correlation analysis by size group: (a) small; (b) middle 1; (c) middle 2; (d) large.

Generally, the AVI detection rate was high when the particle size was small. The relationship between the particle size and the particle defect rate for all size groups is presented in Fig. 6.

Table 2. Correlation analysis by particle group.

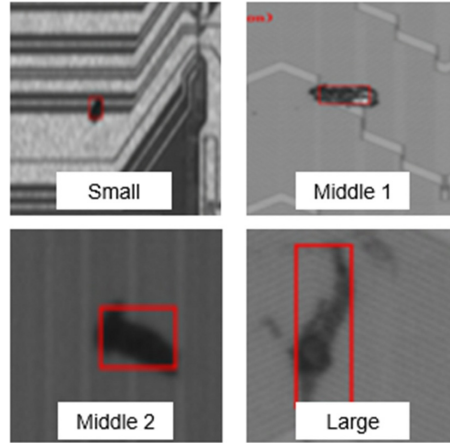|	Small	Middle 1	Middle 2	Large
R^2	0.15	0.73	0.49	0.07
y-intercept	270	90.9	177	354
Slope	0.0489	0.1918	0.4248	0.2847

Fig. 8. Representative images for particle groups.

We have separated the graphs for each particle size group for clarity and further analysis.

As shown in Fig. 7, we have plotted the particle defect rate versus the AVI detection rate for each particle size group. We attempted to determine the extent of association of wire bonding defects with particle size group. We also endeavored to understand why such associations exist or do not exist. We carried out a correlation analysis for each particle size group to assess the relationships. Linear regression analysis is used because it enables establishing size criteria for particle monitoring using our AVI equipment by identifying the particle size groups with high correlation through correlation analysis. Size groups with low correlation are improved with appropriate calibration, enhanced recognition process, and rigorous comparison of correlations between particle types.

First, the correlation between the particle defect rate and the AVI detection rate was obtained for different sizes. As shown in Table 2, the R^2 (coefficient of determination) of the small size group (20–50 μm) was 0.15; 0.73 for the middle 1 size group (50–100 μm); 0.49 for the middle 2 size group (100–150 μm). For the large size group (150 μm ~), the R^2 was 0.07. The highest correlation was observed in the middle 1 size group, whereas the lowest correlation was found in the large size group. For the middle 1 size group, the y-interception was the lowest at 90.9. In addition, R^2 was the highest at 0.73, indicating that the correlation was the strongest for the middle 1 size group.

The representative images for each size group are shown in Fig. 8. The particles in the small size group (20–50 μm), middle 1 size group (50–100 μm), middle 2 size group (100–150 μm), and large size group (150 μm ~) were found to be of various
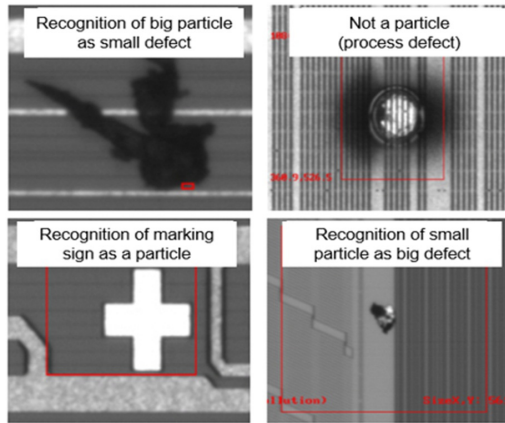
Fig. 9. Typical images of inaccurate recognition by AVI equipment.

shapes. Thus, determining the exact type of particles from the images was difficult. Additional analysis was conducted to understand why such differences in correlation occurred.

3.3 Analysis of size groups with low correlation

We conducted an analysis to determine why low correlation was found in the small and the large size groups compared with the middle 1 and the middle 2 size groups. The result showed that the low correlation in the large size group was primarily due to misidentification by the AVI equipment. As shown in Fig. 9, four types of misidentifications were observed. First, the actual particle size was large, but the AVI equipment recognized it as small. Second, non-particles were inaccurately identified as particles. Third, surface marking signs were incorrectly identified as particles. Lastly, the actual particle size was small, but the AVI equipment recognized it as a large particle. The chip surface has various intrinsic unknown patterns. The intrinsic patterns are occasionally misrecognized as a large particle because our AVI equipment recognizes particles from the reflection of light shed on the chip surface. Thus, the correlation was found to be low for the large size group.

3.4 Analysis of size groups with high correlation

We conducted an analysis to understand the high correlation in the middle 1 size group ranging from 50 μm to 100 μm. Prior to this study, no misidentifications by the AVI equipment have been recorded, and all particles were accurately detected, except for cases with low correlation. To delve deeper into the analysis, we separated the middle 1 size group particle defect rates by the chip pad and the substrate pad positions and performed a correlation analysis. The results showed that the correlation at the substrate pad position had an R^2 value of 0.77, whereas the correlation at the chip pad position had an R^2 value of 0.46. To understand this finding, we attempted to elucidate the pathway by intentionally contaminating 50 μm
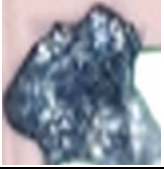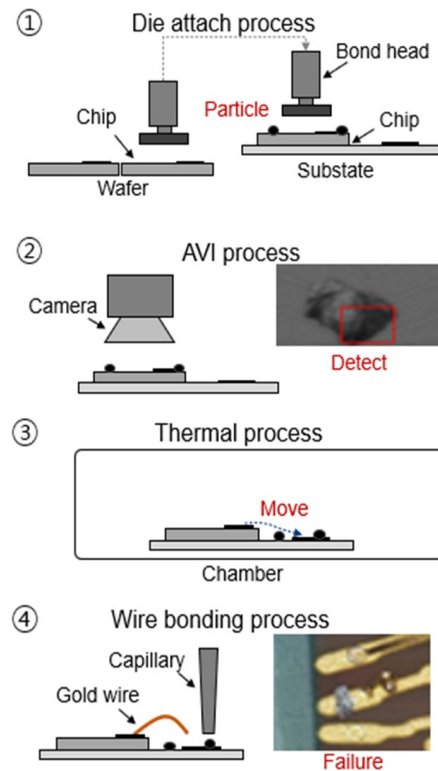

Fig. 10. Plausible pathway of particle defect in wire bonding.

particles and working through the same process.

As shown in Fig. 10, we analyzed the die attach process and wire bonding. Our analysis revealed that the contamination on the chip area was due to particles falling from the internal components, such as the bond head of the equipment, caused by friction and wear. We deliberately increased this contamination and conducted inspections using a camera during the subsequent AVI process. We captured images and attachment locations for each particle. During the following thermal process, the chip was introduced into the chamber, and the temperature typically increased above 100 °C. During this phase, particle movement occurred. Then, the particles, which were originally supposed to adhere to the chip, were transported beneath the chip due to the thermal effects, and some of them adhered to the substrate pad positions. As a result, during wire bonding, the gold wire connections failed due to the presence of particles on the substrate pad positions. This particle defects led to failure. Through this approach, we understand the difference in correlation between the chip pad (R^2 = 0.46) and the substrate pad (R^2 = 0.77).

We examined the materials, types, and occurrence rates of particle defects in the wire bonding process. As shown in Table 3, the majority of particle defects were aluminum, accounting for approximately 80 % of the total defects. Human skin particles constituted 14 %, grease particles 2 %, and the remaining 4 % was composed of other origins. Aluminum and human skin particles are airborne particles. In the thermal process, the temperature of the chip surface increased above 100 °C due to

Table 3. Analysis results by particle type.

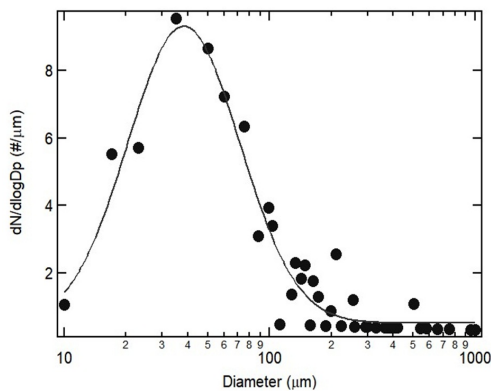| Actual images	Materials observed	Type	Share
	Aluminum	Airborne particle	80 %
	Human skin	Airborne particle	14 %
	Grease	Sticky particle	2 %
ETC.			4 %

Fig. 11. Size distribution of particle defect.

heat. In a cooling zone of the thermal process, cool air was blown onto the chip. Thus, the temperature was different between the chip surface and the air. Buoyancy may lift particles, such as aluminum and human skin due to the natural convection. Moreover, these particles move due to the air blow velocity and then easily settle in the downward direction under the influence of gravity. Consequently, the prevalence of airborne particles indicates that particle movement to the substrate pad occurred easily during the thermal process.

We measured the diameters of particle defects generated during the wire bonding process. The arithmetic mean size was 124 μm, and particle defects were concentrated around 45 μm, as shown in Fig. 11. Particles primarily migrate to the substrate pad due to thermal processes, leading to defects during wire bonding on the substrate pad. Furthermore, utilizing AVI equipment for particle monitoring in semiconductor packaging wire bonding is highly appropriate [13]. Although some differences may be observed based on structural design of the semicon-

ductor packaging, establishing a size criterion of approximately 50 μm to 100 μm and monitoring particles accordingly would be highly effective in controlling contamination particles.

The AVI system can be applied not only to semiconductor environments but also to other harsh environments for identifying and monitoring small particles, such as black carbon. The size of black carbon can range from tens of nanometer to tens of micrometers when the primary black carbon particle is aggregated in the atmosphere [14, 15]. Considering that the AVI can detect particles as small as tens of micrometers, atmospheric black carbon aggregate particles can be identified.

4. Conclusion

In this study, we investigated particle defects observed in the wire bonding process, a critical step of semiconductor package manufacturing. We examined the correlations between the particle defect rate and the AVI detection rate using the AVI system. Moreover, we categorized contamination particles into the small size group (20–50 μm), the middle 1 size group (50–100 μm), the middle 2 size group (100–150 μm), and the large size group (larger than 150 μm) based on the particle sizes detected by our AVI, considering the diameter of gold wire and the widths of a chip pad as well as a substrate pad.

The R^2 between the particle defect rate and the AVI detection rate was 0.15 for the small size group (20–50 μm), 0.73 for the middle 1 size group (50–100 μm), and 0.49 for the middle 2 size group (100–150 μm). However, the R^2 for the large size group was the lowest at 0.07. The examination of images of particle defects showed that the low correlation in the small and large groups was due to the inaccurate recognition by the AVI equipment. The chip surface has various intrinsic unknown patterns. Our AVI equipment recognized particles from the reflection of light on the chip surface. Therefore, intrinsic patterns on the surface were misrecognized sometimes because of the large contamination particles. This technique should be improved for better detection of contamination particles in the future.

To analyze the high-correlation size groups, we evaluated process reproducibility. Particles generated from friction and wear of the equipment in the die attach process were likely to move onto the chip area, causing particle defect. These particles adhered to the chip and the substrate due to natural convection caused by temperature difference between the substrate and the air during the thermal process, leading to failure during wire bonding. This finding resulted in differences in the coefficient of determination for the chip pad position (R^2 = 0.46) and the substrate pad position (R^2 = 0.77). In addition, the arithmetic average size and the modal size of particle defect was approximately 124 and 45 μm in wire bonding, respectively.

For effective contamination control through particle monitoring using AVI equipment, a standard size criterion, approximately 50 μm to 100 μm must be established, although slight variations may exist across different product designs.

To the best of our knowledge, this study showed for the first time that particle defects were related to thermal process in the semiconductor packaging process. However, a further study is required to fully understand the mechanism of generation, growth, transport, attachment, and removal of contamination particles in thermal processes.

Acknowledgments

Nomenclature

ε : Particle defect rate
μ : Number of wire bonding defective particles
γ : Wire bonding population parameter
α : AVI detection rate
ρ : Number of AVI detected particles
β : AVI population parameter
R^2 : Coefficient of determination

References

[1] T. S. Jeong, J. M. Kim, C. W. Lee and Y. B. Park, Effect of PCB surface finishs on intermetallic compound growth kinetics of Sn-3.0 Ag-0.5 Cu solder bump, *Journal of the Microelectronics and Packaging Society*, 17 (1) (2010) 81-88.

[2] S. M. Hyun and C. W. Lee, TSV core technology for 3D IC packaging, *Journal of Welding and Joining*, 27 (3) (2009) 4-9.

[3] H. Emi, N. Namiki and Y. Otani, Removal of fine particles from smooth flat surfaces by consecutive pulse air jets, *Aerosol Science and Technology*, 23 (4) (1995) 665-673.

[4] J. S. Park and J. Lee, A study on the effect of air jet on particle cleaning at wafer surface, *Transactions of the Korean Society of Mechanical Engineers B*, 44 (9) (2020) 583-590.

[5] K. C. Noh, H. C. Lee, D. Y. Kim and M. E. Oh, Method of particle contamination control for yield enhancement in the cleanroom, *Transactions of the Korean Society of Mechanical Engineers B*, 31 (6) (2007) 522-530.

[6] J. S. Park and J. Lee, Analysis of the type of particle defects in the manufacture of high bandwidth memory using deep learning, *Transactions of the Korean Society of Mechanical Engineers - B*, 47 (7) (2023) 359-366.

[7] K. Kim, K. Kang and S. Jung, Non-destructive evaluation of semiconductor package by electronic speckle pattern interferometry, *Journal of Mechanical Science and Technology,* 19 (2005) 820-825.

[8] S. W. Lee and H. K. Lee, Data acquisition system of compound semiconductor fabrication, *Journal of Mechanical Science and Technology*, 21 (2007) 2149-2158.

[9] M. R. DeYong, T. C. Eskridge, J. W, Grace, J. E, Newberry, J. H, Jones and B. E. Hart, Automated visual inspection stations for next-generation semiconductor package quality control, *Optical Characterization Techniques for High-Performance Microelectronic Device Manufacturing III*, 2877 (1996) 99-110.

[10] P. H. Tsao and A. S. Voloshin, Manufacturing stresses in the die due to the die-attach process, *IEEE Transactions on Components, Packaging, and Manufacturing Technology*, 18 (1) (1995) 201-205.

[11] K. Suzuki, T. Higashino, K. Tsubosaki, K. Mine and K. Nakayoshi, Development of low elastic modulus die attach material and clean cure process, *40th Conference Proceedings on Electronic Components and Technology*, Las Vegas, USA (1990) 835-839.

[12] L. T. Nguyen, D. McDonald, A. R. Danker and P. Ng, Optimization of copper wire bonding on Al-Cu metallization, *IEEE Transactions on Components, Packaging, and Manufacturing Technology*, 18 (2) (1995) 423-429.

[13] J. C. H. Pan and D. H. Tai, A new strategy for defect inspection by the virtual inspection in semiconductor wafer fabrication, *Computers & Industrial Engineering*, 60 (1) (2011) 16-24.

[14] B. Jeong and J. Lee, Effective density and light absorption cross section of black carbon generated in a spark discharger, *Journal of Aerosol Science*, 107 (2017) 55-64.

[15] Y. Cha, S. Lee and J. Lee, Measurement of black carbon concentration and comparison with PM_{10} and $PM_{2.5}$ concentrations monitored at the Chungcheong Province in Korea, *Aerosol and Air Quality Research*, 19 (3) (2019) 541-571.

Joonsub Park is a doctoral candidate pursuing a Ph.D. degree in Mechanical Engineering at the Graduate School of Korea University of Technology. He received his M.S. degree in Mechanical Engineering from the Graduate School of Korea University of Technology and Education. He received his B.S. degree in Mechatronics and IT Convergence Engineering from the Korea University of Technology and Education. His current research area is mainly on the analysis of defects in semiconductor packaging processes.
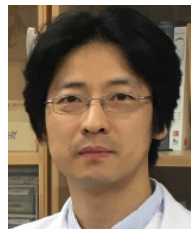
Jeonghoon Lee is a Professor of School of Mechanical Engineering, Korea University of Technology and Education. He received his Ph.D. degree in the School of Mechanical Engineering from Seoul National University in Korea. He received his M.S. degree in the School of Mechanical Engineering from Seoul National University in Korea. He received his B.S. degree in the Department of Mechanical Engineering from Seoul National University in Korea. His research area includes aerosol particle technology, instrumentation for optical measurement, atmospheric aerosol, semiconductor process, and diesel engines.